Combustion characteristics of n-heptane spray combustion in a low temperature reform gas/air environment

Zhong, Shenghui; Xu, Shijie; Bai, Xue-Song; Hadadpour, Ahmad; Jangi, Mehdi; Zhang, Fan; Du, Qing; Peng, Zhijun

DOI:
10.1016/j.fuel.2021.120377

Combustion characteristics of n-heptane spray combustion in a low temperature reform gas/air environment

Shenghui Zhong[a,b], Shijie Xu[b], Xue-Song Bai[b,*], Ahmad Hadadpour[b], Mehdi Jangi[c], Fan Zhang[a,**], Qing Du[a], Zhijun Peng[a]

[a]*State Key Laboratory of Engines, Tianjin University, 135 Yaguan Rd, 300350 Tianjin, China*
[b]*Department of Energy Sciences, Lund University, 22100 Lund, Sweden*
[c]*Department of Mechanical Engineering, University of Birmingham, B15 2TT Birmingham, United Kingdom*

Abstract

This paper presents a large eddy simulation study of n-heptane spray combustion in an n-heptane low temperature reform (LTR) gas environment in a constant volume combustion chamber, under conditions relevant to single-fuel reactivity controlled compression ignition (RCCI) combustion engines. The LTR gas is made up of partially oxidized intermediate species from rich n-heptane/air mixture in an external constant temperature reformer. It is found that a higher reform temperature results in a longer ignition delay time of the n-heptane spray and a higher liftoff length, due to the chemical effect of the LTR gas and the difference in the reaction zone structures. A significantly different spray flame structure is identified in the RCCI case from that of single-fuel spray combustion. After the onset of high temperature ignition, a double-layer flame structure is established in the RCCI

*Corresponding author.
E-mail address: Xue-Song.Bai@energy.lth.se
**Corresponding author.
E-mail address: fanzhang_lund@tju.edu.cn

case, with a diffusion flame layer and a lean premixed flame layer. The lean premixed flame affects the flow field, which significantly suppresses the mixing around the spray tip. As a result, the RCCI case exhibits a lower NOx formation but a higher soot formation than the single-fuel case.

Keywords: spray combustion, fuel reform, dual fuel, Engine Combustion Network, Eulerian stochastic fields

1. Introduction

To reduce the impact of greenhouse gas and pollutant emissions from internal combustion engines (ICE) on the environment, intensive research has been carried out on developing advanced ICE combustion concepts [1–5]. The use of reform gas is one novel approach [2], in which the exhaust gas heat can be used to reform the fuel to smaller hydrocarbons and syngas (CO and H_2), by which the engine exhaust heat can be recovered in the endothermic fuel reform reactions and the engine efficiency can be improved. Tsolakis *et al.* [6] investigated exhaust gas assisted fuel reform in diesel engines and reported that diesel fuel can be reformed to LTR gases consisting of a high amount of H_2 (up to 16%) at the exhaust gas temperature of 563 K with the assistance of a metal catalyst. It was shown that when the engine exhaust gas recirculation (EGR) was replaced by the LTR gases the engine-out emissions of soot and nitrogen oxides (NOx) could be reduced. Alger and Mangold [7] demonstrated an onboard reform approach to generate a "dedicated EGR" in a spark-ignition gasoline engine, in which one of four engine cylinders was used to generate the EGR under fuel-rich conditions. The EGR was then used in the other three cylinders, which resulted in a significant improvement of the fuel efficiency (by 10% at light load) and a significantly decreased CO and

unburned hydrocarbon (UHC) emissions, due to the existence of H_2 in the EGR that enhanced near-wall combustion [7].

Dual-fuel Reactivity controlled compression ignition (RCCI) is another novel advanced engine combustion concept [1, 8], which has the potential to achieve simultaneously high engine efficiency and low emissions. In RCCI engines, a low reactivity fuel is introduced into the cylinder to create a well-mixed charge of low reactivity fuel, air and EGR. A high reactivity fuel is then injected before ignition of the low reactivity fuel. RCCI engines suffer from the high sensitivity of ignition delay time (IDT) to the incylinder charge conditions, and as such, the control of ignition and heat release rate poses a challenge. This challenge could be mitigated by combining the potential of both RCCI and reform gas [3, 9]. Geng *et al.* [3] investigated a low temperature "single-fuel" RCCI engine. The fuel (n-heptane) was reformed in an external reformer, under fuel-rich conditions, through low temperature ignition reactions without the assistance of a catalyst. The reform gas was introduced into the engine cylinder via the intake port where it was cooled by mixing with intake air. Thus, the single-fuel RCCI process is conceptually similar to that of dual-fuel RCCI, while it has the advantage of without having to use two fuel tanks. In the baseline case of Geng *et al.* [3], the reformer temperature was set to 423 K, under which the n-heptane in the reformer was vaporized but not reformed. Thus, the end gas from the reformer was a mixture of gaseous n-heptane and air. Compared with the baseline unreformed case, the reform gas case exhibited a longer IDT, a lower heat release rate (HRR) and a lower soot emission. These latter two properties are advantageous for the engine performance at high load operation conditions, where the high values of peak HRR and soot emission are of concern.

The fundamental physics behind the longer IDT, lower HRR and soot formation in the reform gas single-fuel RCCI engine is unclear. It is expected that this is a result of the LTR gas chemistry, e.g., the absence of the low temperature ignition path in the LTR gas (that exists in the parent fuel, e.g., n-heptane), and the change of the reaction front structure. The basic process of single-fuel RCCI combustion can be identified to consist of three stages [10–12]: (a) onset of ignition in the mixing layer of the directly injected fuel and the earlier injected reform gas/air mixture (premixed charge), (b) reaction front propagation in the earlier injected reform gas/air mixture, which can be either in the ignition wave mode or in the premixed flame mode, and (c) combustion of the fuel-rich mixture of the directly injected fuel in a diffusion flame mode. A recent experiment of Srna *et al*. [13] on n-dodecane/methane RCCI combustion illustrated the transition process between the different stages. Their results showed that a considerable amount of the directly injected fuel (n-dodecane) was consumed in a flame-like propagation mode in the mixing layer of n-dodecane and the surrounding lean premixed methane/air mixture, followed by a premixed flame-like propagation in the lean premixed methane/air mixture.

The combustion process of an n-heptane spray in a lean premixed n-heptane LTR gas/air ambient environment in a constant volume chamber, under conditions relevant to the single-fuel RCCI engine of Geng *et al*. [3], is studied in the present work. The aim is to gain an improved understanding of (a) the effect of LTR gas on the ignition of the parent fuel, (b) the structure of the reaction fronts in the mixing layer of the directly injected parent fuel and the LTR gas, and in the ambient lean LTR gas/air mixture, and (c) the NOx and soot formation process in LTR gas RCCI combustion. Since the RCCI combustion process involves multiple

modes, we chose to use large eddy simulation (LES) coupled with a finite rate chemistry approach. This approach has been used to study spray combustion in ambient methane/air mixtures [14, 15]. The approach offers detailed data for the analysis of chemical reaction paths toward ignition and NOx/soot formation, and for identification of the reaction front structures.

2. Numerical Method

A transported probability density function (PDF) is employed to model the sub-grid scale (SGS) turbulence/chemistry interaction in the gas phase combustion process. A Lagrangian particle tracking approach is used to model the liquid spray, and the mass, momentum and heat transfers between the gas and liquid phases are modeled using source terms in gas and liquid phase transport equations. Liquid n-heptane is injected as spherical droplets, with the initial droplet size following the Rosin-Rammler distribution [16]. Following previous works [17, 18], the mean diameter of droplets is set as a half of the injector nozzle diameter, while the maximum size is set as the diameter of the injector nozzle. The secondary break-up process is modeled using a hybrid Kelvin Helmholtz-Rayleigh Taylor (KH-RT) model [19]. The Frossling model and the Ranz-Marshall correlation are employed to describe the droplet evaporation and heat transfer with the surrounding gas phase, respectively. A detailed description of the spray sub-models for atomization, breakup and evaporation is given in Ref. [20].

The PDF transport equations are solved using an Eulerian stochastic fields (ESF) method [21]. In the ESF method, the mean and moments of a random vector $\phi = (\phi_1, \phi_2 \cdots \phi_{N_s+1})$ are approximated by N_F number of stochastic fields, $\xi_\alpha^{(n)}$, where the vector ϕ represents the N_s number of chemical species (species

mass fractions) and the mixture enthalpy. $\widetilde{\phi}_\alpha = \frac{1}{N_F}\sum_{n=1}^{N_F}\xi_\alpha^{(n)}(\mathbf{x},t)$. The equation for the n^{th} stochastic field is:

$$\overline{\rho}d\xi_\alpha^{(n)} = C + D + M + W + S \tag{1}$$

where

$$C = -\frac{\partial\overline{\rho}\tilde{u}_i\xi_\alpha^{(n)}}{\partial x_i}dt, D = \frac{\partial}{\partial x_i}\left(\Gamma_t\frac{\partial\xi_\alpha^{(n)}}{\partial x_i}\right)dt,$$

$$M = -\frac{1}{2}\overline{\rho}C_\phi\left(\xi_\alpha^{(n)} - \widetilde{\phi}_\alpha\right)\omega^{sgs}dt, W = \overline{\rho}\sqrt{2\frac{\Gamma_t}{\overline{\rho}}}\frac{\partial\xi_\alpha^{(n)}}{\partial x_i}d^{(n)},$$

$$S = \overline{\rho}S_\alpha^r\left(\xi^{(n)}\right)dt + \overline{\rho}S_\alpha^s\left(\xi^{(n)}\right)dt \tag{2}$$

with $1 \leq \alpha \leq \mathrm{N}_s + 1$ and $1 \leq n \leq \mathrm{N}_F$.

The above equation implies invoking the gradient transport hypothesis to model the turbulent eddy transport fluxes. Here Γ_t is the sum of total molecular and sub-grid scale diffusivities. $\overline{\rho}S_\alpha^r\left(\xi^{(n)}\right)dt$ and $\overline{\rho}S_\alpha^s\left(\xi^{(n)}\right)dt$ are the increment in $\xi_\alpha^{(n)}$ due to chemical reactions and spray injection, respectively. $\overline{\rho}$ is the filtered gas density. C_ϕ is set to 2, which is a model constant in the micro-mixing model IEM (interaction with exchange to the mean) [22]. ω^{sgs} is the SGS scalar turbulent frequency, $\omega^{sgs} = \frac{\mu+\mu^{sgs}}{\overline{\rho}\Delta^2}$, with Δ being the filter width modeled as the cube root of the volume of the mesh cell. μ and μ^{sgs} are the laminar and SGS viscosity, respectively. The SGS diffusivity is modeled by one equation eddy-viscosity model. $d^{(n)}$ is approximated by time-step increments $dt^{1/2}\eta_i^n$, where η_i^n is a $\{-1,1\}$ dichotomic random vector [21]. The random vector η_i^n is independent of space but different for each field. A factorization scheme [23] with three steps is adopted to solve the stochastic fields equation. Specifically, Step 1 involves the process of convection, diffusion, spray and Wiener term:

$$\overline{\rho} d\xi_{\alpha}^{(n)} = C + D + W + \overline{\rho} S_{\alpha}^{s}\left(\xi^{(n)}\right) dt \tag{3}$$

Step 2 is the micro-mixing process with analytical solution:

$$\xi_{\alpha}^{(n)} = \widetilde{\phi_{\alpha}} + \left(\xi_{\alpha}^{(n)} - \widetilde{\phi_{\alpha}}\right) * \exp\left(\omega^{sgs} dt\right) \tag{4}$$

The final step deals with the integration of the chemical reaction rates. To reduce the computational time of this step, the chemistry coordinate mapping (CCM) [24] acceleration method is coupled with the stiff ordinary differential equation (ODE) solver Seulex [25]:

$$\xi_{\alpha}^{(n)} = \xi_{\alpha}^{(n)} + S_{\alpha}^{r}\left(\xi^{(n)}\right) dt \tag{5}$$

The CCM phase space variables are temperature $T^{(n)}$, equivalence ratio $\Phi^{(n)}$, scalar dissipation rate $\chi^{(n)}$, fuel mass fraction $Y_{fuel}^{(n)}$, and a fuel mass ratio of spray injection $\lambda_{fuel}^{(n)}$. The former four dimensions were adopted to describe the reaction progress, the fuel stratification, the mixing rate and the reaction progress in low temperature ignition [18]. The fifth variable, $\lambda_{fuel}^{(n)}$, is introduced to describe the mixing between the injected fuel and ambient LTR fuel. $\lambda_{fuel}^{(n)}$ is defined based on the mole numbers of C and H atoms:

$$\lambda_{fuel}^{(n)} = \frac{\widetilde{Z} * \left(4n_{\mathrm{C,fuel}} + n_{\mathrm{H,fuel}}\right)}{\sum_{i=0}^{N_s} Y_i^{(\mathrm{n})}(4n_{\mathrm{C,i}} + n_{\mathrm{H,i}})} \tag{6}$$

where $\widetilde{Z}$ is the mixture fraction, obtained from a transport equation:

$$\frac{\partial \overline{\rho}\widetilde{Z}}{\partial t} + \frac{\partial \overline{\rho}\tilde{u}_i\widetilde{Z}}{\partial x_i} = \frac{\partial}{\partial x_i}\left(\overline{\rho}\Gamma_t\frac{\partial \widetilde{Z}}{\partial x_i}\right) + \overline{\rho}S_{\mathrm{fuel}}^{S} \tag{7}$$

where $\overline{\rho}S_{\mathrm{fuel}}^{S}$ is the source term from the liquid n-heptane injection. $\widetilde{Z} = 1$ indicates the condition of pure n-heptane vapour in the mixture, whereas $\widetilde{Z} = 0$ indicates

the LTR gas/air ambient mixture. The CCM method was shown to have a speedup rate of at least a factor of ten.

The n-heptane chemical mechanism of Lu *et al.* [26], which includes 68 species and 283 elementary reactions, is employed to describe the reform process and spray combustion. The extended Zeldovich mechanism [27] is coupled with the Lu *et al.* mechanism to predict the formation of NOx. The multistep soot model of Leung *et al.* [28] is used to predict the soot formation. The open-source CFD code, OpenFOAM 4.x [29], is used in the LES. A finite volume method with a second-order scheme is adopted for the spatial discretization and an implicit second-order backward Euler scheme is used for the time integration. Eight stochastic fields are used to capture the SGS PDF distributions, which have been proven to provide reasonable accuracy [23] at an affordable computational cost.

3. Case Specifications

The computational cases were selected according to the experiments of Geng *et al.* [3]. The n-heptane/air LTR process took place in a constant temperature channel reformer under atmospheric pressure with a residence time of 17.2 s, an equivalence ratio of 8, and three reform temperatures (T_r) of 450 K, 550 K and 650 K. The reform process was modeled as a homogeneous reactor using the Lu *et al.* mechanism [26]. The parent fuel conversion rate (FCR) and the mass fractions of key species from the reformer are given in Table 1. The full list of species mass fractions of LTR products is provided in the Supplementary data. After LTR, the mixture was quickly cooled to 349 K, and the LTR gas was mixed with air to form an LTR gas/air mixture with an equivalence ratio of 0.3. Case 1 acts as

a validation case for the present spray combustion model, and also as a baseline reference case for the n-heptane spray combustion. Specifically, the ambient air in Case 1 has a temperature of 900 K, an initial pressure of 40 bar, a density of 14.8 kg/m^3, and a mole fraction of oxygen of 21%. The fuel injector nozzle is 100 μm with 150 MPa injection pressure and 6.8 ms injection time. This case is known as the Engine Combustion network (ECN) Spray-H and well-documented experiments are available [30]. Cases 2, 3, and 4 are LTR gas RCCI cases with the same combustor and injector configuration, and ambient gas temperature, as in Case 1, but with three different reform temperatures. Case 5 has the same reform temperature as Case 4, but with an ambient equivalence ratio (Φ_a) of 0.5. The ambient pressure is slightly different from Case 1, to maintain the same density of 14.8 kg/m^3. The computational domain is a cube with a side length of 108 mm, which is the same as the ECN rig [30]. The LES mesh is locally refined to 0.25 mm in the near injector region where spray evaporation, ignition and earlier flame propagation take place. It is shown that the chosen grid yields a grid-independent result, and the ignition and liftoff process of the n-heptane spray flame are captured very well [17, 31]. The CFL number is limited to 0.1, resulting in a time step of approximately 5×10^{-8} s, which is enough to capture the unsteady motion of spray combustion.

4. Results and Discussions

4.1. Model Validation

The non-reacting spray ECN Spray-H experiments [30] is studied to validate the spray model. This case is referred here to as Case NR, which has an initial ambient temperature of 1000 K with zero oxygen in the ambient mixture [30].

Table 1: Case setup and mass fractions of representative species of the reform gas.

Case	$T_r(K)$	FCR (%)	NC_7H_{16}	NC_7KET	CH_2O	CO	Φ_a	T_α (K)	ρ_α (kg/m^3)
1	-	-	0	0	0	0	0	900	14.8
2	450	0	0.3466	0	0	0	0.3	900	14.8
3	550	82	0.0611	0.0060	0.0088	0.0353	0.3	900	14.8
4	650	88	0.0412	0	0.0075	0.0482	0.3	900	14.8
5	650	88	0.0412	0	0.0075	0.0482	0.5	900	14.8

The initial pressure conditions and the spray setups are the same as that in Case 1, Table 1. Figure 1 shows a comparison between the measured and the predicted liquid and vapor penetration lengths and radial profiles of mixture fraction. The liquid length is defined as the farthest axial distance with 5% liquid volume and the gas penetration is the maximum distance from the nozzle outlet to where the mixture fraction is 0.1% [30]. All these quantities predicted in LES are in good agreement with experimental data, cf. Fig. 1.

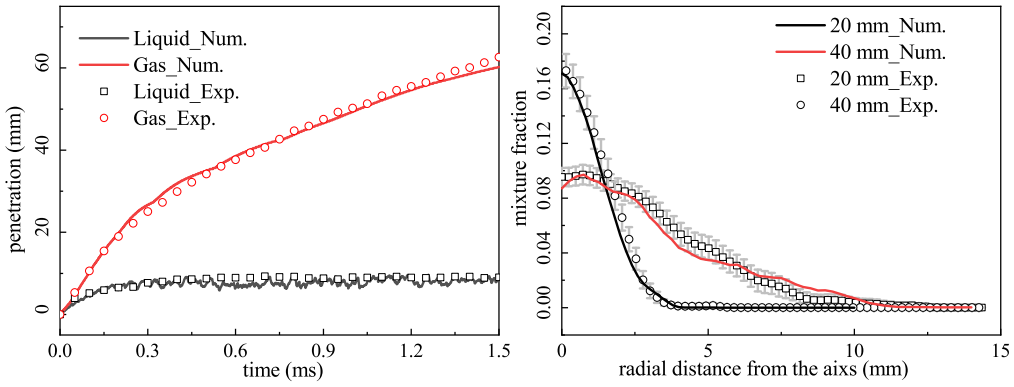

Figure 1: Lquid and gas penetration in the non-reacting case (left). Mixture fraction spatial distribution along the radius direction at two axial height of the non-reacting case (right). Symbols represent the ECN experimental results [30] and lines are the LES results.

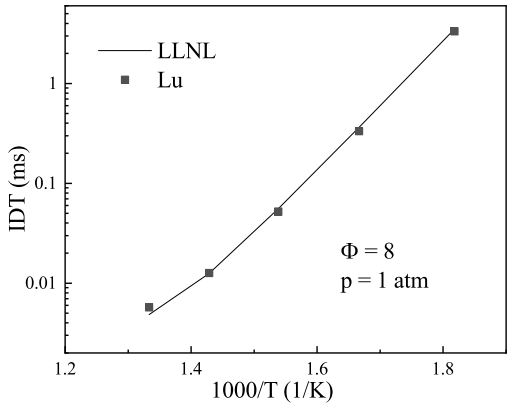

Figure 2: Predicted ignition delay time (IDT) of rich n-heptane/air mixture (Φ = 8) using the Lu *et al.* mechanism and the LLNL mechanism under different initial temperatures and atmospheric pressure.

The performance of Lu *et al.* mechanism is examined under current fuel rich condition. Lu *et al.* mechanism is a skeletal mechanism based on the detailed LLNL n-heptane mechanism (version 2) [32] and it has been used in n-heptane spray combustion simulation [33]. Since the reform process is governed by the low temperature reaction path of n-heptane chemistry, and Lu *et al.* mechanism is validated against the detailed mechanism under the current reform condition ($\Phi = 8$). As seen in Fig. 2, the ignition delay time (IDT) predicted by Lu *et al.* mechanism is nearly the same as that by the detailed mechanism.

To validate the ESF model and the dependence of the results on the number of stochastic fields (N_F), the pressure rise history predicted using different N_F is compared with ECN experiments and LES predictions by the well-stirred reactor (WSR) model. WSR has been used in recent LES of n-dodecane spray flames [14]. Much finer grid may be needed with WSR (with one fourth of the current mesh size). With the current grid resolution, the pressure rise is significantly under-

predicted with WSR compared with ESF regardless the number of stochastic fields. Note that this is consistent with the results of Som *et al.* [33], in which similar LES filter size and mesh size were used. It was shown that Lu *et al.* mechanism with WSR always predicted a longer IDT. When increasing the number of stochastic fields from two to twelve, it is shown that the pressure rise profile converges, cf. Fig. 3. Marginal differences are found between the results from the eight and twelve stochastic fields for the onset time of pressure rise, and the slope of pressure rise profile.

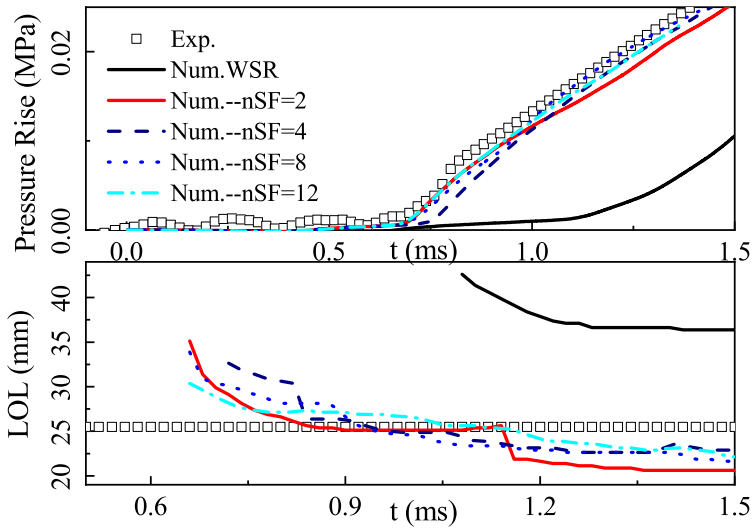

Figure 3: Temporal evolution of mean pressure (top) and liftoff length (bottom) in the combustor of Case 1 with different number of stochastic fields. Symbols represent the ECN experimental results [30] and lines are the LES results.

Figure 3 shows also comparison of measured and predicted liftoff length (LOL) with different models and N_F. Here, LOL is defined as the nearest axis distance, where OH mass fraction reaching its 2% of the maximum value [30]. The results are consistent with the pressure rise. The WSR model over-predicted the LOL,

while the ESF model yields a better prediction of LOL. The predicted LOL converges as N_F increases from 2 to 12. In the following simulations eight stochastic fields are adopted as a compromise between accuracy and CPU time.

The validation of the soot model has been done for an n-heptane spray flame case similar to Case 1 (with a different ambient temperature of 1000 K). The results were presented in our previous work [34]. The temporal evolution of experimental and LES predicted soot optical thickness were compared at axial locations of 40 mm, 50 mm and 60 mm downstream the injector nozzle exit plane. The line-of-sight extinction (KL) data were measured using Laser-induced incandescence (LII), while the LES predicted KL was converted from the spatial integration of soot volume fraction as suggested by ECN [30]. The onset of the soot formation and the magnitude of KL value were well-predicted in the current LES model.

Fig. 4 shows the pressure rise for the Cases 1-4 and the corresponding ECN experimental results for Case 1 [30]. The numerical results are in good agreement with the experimental data, including the ignition delay time and the heat release rate. For the LTR gas RCCI cases, the time at which pressure starts to rise shows a non-monotonic dependence on FCR or reform temperature, whereas the pressure rise rate appears to decrease with increasing FCR or LTR temperature. Further details on the ignition process will be investigated below.

4.2. Ignition and Flame Liftoff

In n-heptane ignition, the low temperature ignition (LTI, also known as cool flame) can be characterized with heptyl-peroxide (RO_2) or ketohydroperoxide (NC_7KET), whereas high temperature ignition (HTI) is associated with a rapid increase in temperature and the concentration of OH radicals. The temporal evolution of the maximal temperature and mean mass fraction of OH radicals,

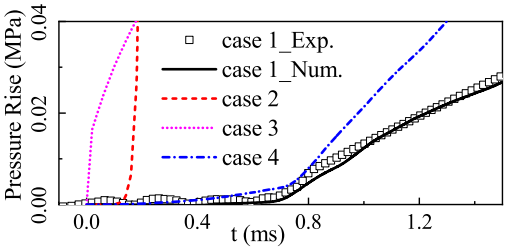

Figure 4: Temporal evolution of pressure in the combustor. Symbols represent the ECN experimental results [30] and lines are the LES results.

displayed in Fig. 5, indicates that the IDT (i.e., τ_{ig}, the time at the onset of HTI) of Case 2 is 0.46 ms, the shortest among all cases. Note that the mean temperature in Fig. 5 is mainly governed by combustion of the ambient gas; thus, the temporal evolution of the mean temperature (TMean) denotes the ambient fuel reactivity, because the injected fuel is much less than the ambient fuel due to the large domain. With the lowest LTR temperature, the ambient gas in Case 2 is a mixture of n-heptane and air. The ambient n-heptane/air mixture has a temperature of 900 K, which, due to the negative temperature coefficient (NTC), gives rise to a longer IDT in the ambient mixture than that in the mixing layer of the ambient gas and the vapor n-heptane from the liquid jet, due to the lower temperature in the mixing layer. The ignition in both the mixing layer and the ambient mixture of Case 2 undergoes two stages, LTI and HTI stages. The LTI stage (the cool flame stage) at 0.2 ms is indicated by the local peak mass fractions of OH, NC_7KET, and RO_2. The heat release from LTI in Case 2 is substantial, resulting in a 40 - 50 K increase in the mean combustor temperature, the highest increase among all cases, along with the highest mean mass fractions of OH, NC_7KET, and RO_2.

The LTR temperature in Case 3 is 550 K, which is high enough to reform the fuel into LTI products, including NC_7KET, with a small amount of unburned

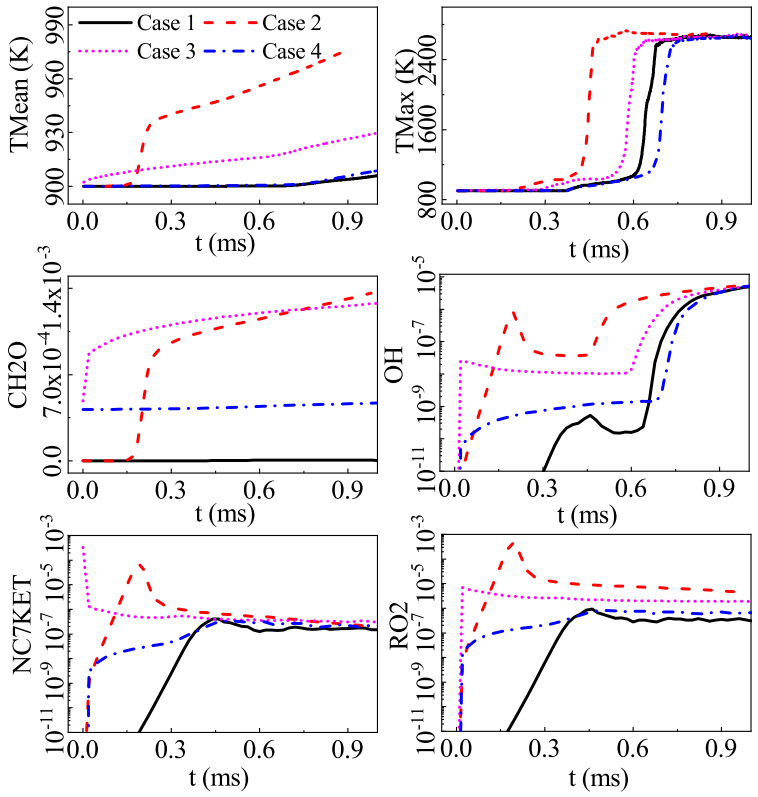

Figure 5: Temporal evolution of mean temperature, maximal temperature, and mean species mass fractions (CH_2O, OH, NC_7KET, RO_2) in the combustor.

n-heptane and a FCR of 82%. The LTI products start to react almost immediately, forming OH radicals (via decomposition of NC_7KET to OH radicals), while also giving rise to a noticeable heat release in the ambient mixture. Due to the large amount of mass in the ambient gas, the mean temperature in the combustor shows an immediate increase, along with an immediate increase of pressure, cf. Figs. 4 and 5. The mixing layer of the ambient gas and the vapor n-heptane from the liquid jet is, however, not as quickly ignited as in Case 2. The lower level of n-heptane in the LTR gas is the reason behind the longer IDT in Case 3 as compared with that

of Case 2, due to the weaker NTC effect. This also explains the longest IDT of Case 4 among all cases, since the case has the highest LTR temperature, thus, the highest FCR, and the lowest mass fraction of n-heptane in the LTR gas, among all cases. Although the mass fractions of OH, NC_7KET and RO_2 are evident shortly after the start of injection, the cool flame is rather weak, as is evident from the nearly constant mean temperature, and mass fractions of CH_2O and OH, before the onset of HTI. In fact, the IDT of Case 4 is even longer than that of Case 1 (a case without any fuel in the ambient gas). The longer IDT with increasing FCR is consistent with the experiments of Geng *et al*. [3].

As the ambient gas Φ increases from 0.3 in Case 4 to 0.5 in Case 5, the inhibiting effect of LTR products on n-heptane ignition is more significant, cf. Fig. 6. Comparing Cases 5 and 4 with Case 1, it is found that the inhibiting effect of LTR products on HTI is more obvious than on LTI. As the LTR products have a lower capability to release heat from low temperature chemistry [35], the maximal temperature increase is rather slow in the transition process from LTI to HTI in Case 5, which delays the HTI [36]. This is consistent with the n-heptane NTC effect. Higher n-heptane level in the mixture leads to stronger NTC effect and higher heat release from low temperature ignition.

Fig. 7 shows the temporal evolution of flame liftoff length, LOL. For all cases, the onset of HTI is at a downstream position, and the ignition fronts propagate upstream with time, giving rise to a decreasing LOL. It is evident that the LTR gas has significant effects on the LOL; a higher FCR leads to a longer LOL. The value of LOL is closely correlated with the value of IDT, i.e., a shorter IDT corresponds to a shorter LOL, indicating that the leading front of the lifted flame is assisted by the ignition reactions upstream the lifted flame [20].

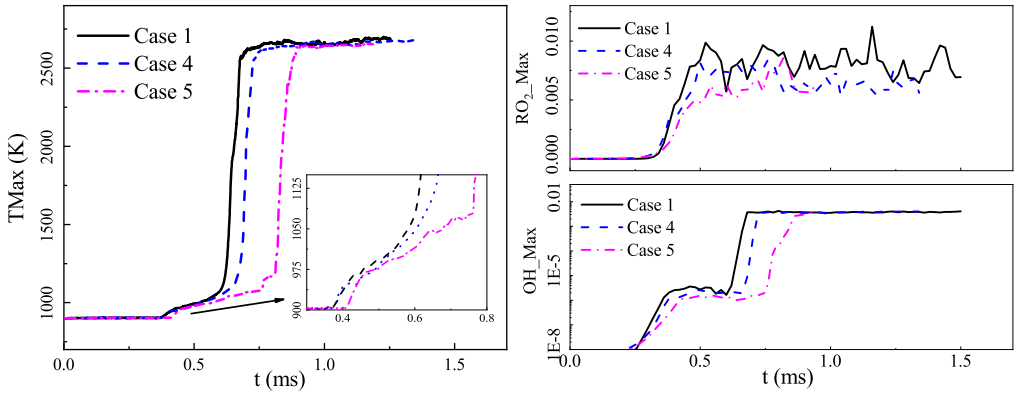

Figure 6: Temporal evolution of maximal temperature and species mass fractions (OH and RO_2) in the combustor for Cases 1, 4 and 5.

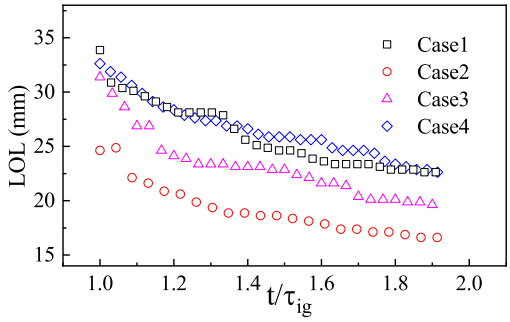

Figure 7: Temporal evolution of LOL. Time is normalized by the value of IDT.

4.3. Flame Structure

Fig. 8 shows a 2D distribution of the instantaneous heat release rate, HRR, after the onset of HTI. Considering that Cases 1 and 4 have a similar IDT and LOL, they are selected and compared here to investigate the effects of ambient LTR gas on the structure of the spray flame. Following the definition of local equivalence ratio (Φ) in Ref. [37], the Φ iso-contour lines shown in Fig. 8 consider the fuels from both the ambient gas and the injected fuel. For both Cases 1 and 4, the onset of HTI (indicated by the high HRR region) occurs in the fuel-rich region at the

spray tip, and a low HRR region from LTI (cool flame) is shown in the upstream region. The HTI fronts propagate upstream towards the LTI region and the HTI and LTI regions merge together at about $1.4\tau_{ig}$.

Downstream of the HTI fronts, a diffusion flame (DF) is formed around the stoichiometric iso-contour line ($\Phi = 1$) with a thin heat release layer, and a lean premixed flame (LPF) is formed in the proximity of the DF in the fuel-lean region. As evident in the time interval from $1.12\tau_{ig}$ to $1.42\tau_{ig}$, the double-layer flame structure propagates downstream, due to continuous injection of the liquid fuel and the penetration of the vapor fuel. As the process is evolving in time, for the single-fuel case, Case 1, the LPF and DF separate each other in space and the LPF is gradually weakened and quenched eventually, once the mass fraction of the fuel vapor in the mixture downstream of the flame is too low to sustain the LPF. In the LTR gas RCCI case, Case 4, the LPF and DF separate in the periphery of the spray but they stay close to each other at the spray tip. The LPF releases considerable heat at $\Phi \sim 0.5$ as it propagates outwards into the ambient gas. The LPF flame is sustained due to the presence of LTR fuels in the ambient mixture.

Two interesting points in Case 4 are worthy of discussion. One is that the LPF layer is at $\Phi \sim 0.5$, instead of the ambient LTR gas/air mixture of $\Phi = 0.3$, indicating that the LPF is maintained both by the injected fuel and the ambient fuel. Another point is that the mixing between the injected fuel and the ambient gas in the RCCI case, Case 4, is slower than that in single-fuel case, Case 1, in the spray tip region. This results in a larger fuel-rich region (enclosed by Φ > 1.5) in the RCCI case. Fig. 9 shows a 2D distribution of mixture fraction at the instance of time of 1.2 ms for both Case 1 and 4. The stoichiometric mixture fraction (Z_{st}) iso-line in Case 4 is at a similar streamwise location to that in Case 1 at the spray

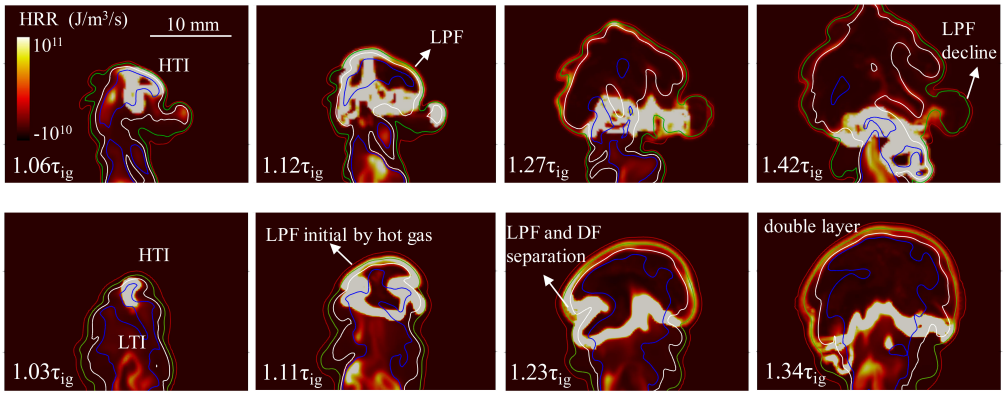

Figure 8: Temporal evolution of heat release rate distribution after high temperature ignition of the spray in Cases 1 (top) and 4 (bottom). Solid blue, white, green and red lines denote the local equivalence ratio 1.5, 1.0, 0.5 and 0.3, respectively.

tip, while the iso-line of $0.5Z_{st}$ at the spray tip in Case 4 is much closer to the iso-line of Z_{st}, than in Case 1. This indicates that the mixing field is influenced by the LPF in the RCCI case, which has a significant impact on the soot emission to be discussed below.

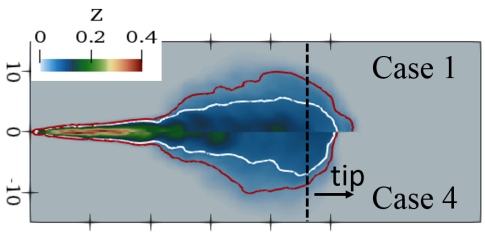

Figure 9: Circumferential averaged mixture fraction distributions at 1.2 ms. Solid white line represents stoichiometric mixture fraction, and solid red line denotes half of stoichiometric mixture fraction.

To explain the poor mixing in the RCCI case, Fig. 10 presents the distribution of Z, HRR and axial velocity, U, along the central axis of the jet. In Case 1, the

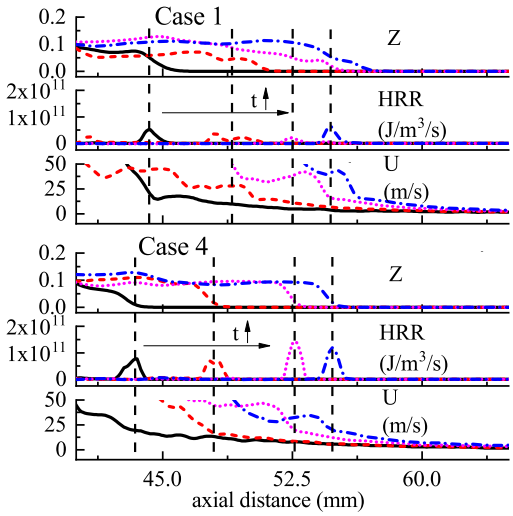

Figure 10: The mixture fraction (Z), heat release rate (HRR) and axis velocity (U) profiles along the central axis line with time evolving. Solid black line: τ_{ig} + 0.16 ms ; red dash line: τ_{ig} + 0.36 ms; magenta dot line: τ_{ig} + 0.56 ms; blue dash dot line: τ_{ig} + 0.64 ms.

HRR peak is around Z_{st}, and the value of HRR is lower than that in the RCCI case, Case 4. The value of U across the HRR layer varies only slightly, which allows the convective transport of the hot products from the flame to the ambient gas downstream, therefore, enhancing the mixing of the hot products with the ambient gas downstream. On the contrary, in the RCCI case, Case 4, the value of HRR is higher, due to the double-layer DF/LPF structure shown in Fig. 8. The peak HRR is at a much lower value of Z, i.e., $Z < Z_{st}$. The value of U across the HRR layer decreases rapidly. This slows down the convective transport of the hot gas from the flame to the ambient mixture downstream, resulting in a high gradient of mixture fraction in Case 4, cf. Fig. 9. The rapid decrease of U across the LPF is a result of pressure loss across the LPF, from the ambient mixture side towards the DF side. This results in a strong negative pressure gradient along the axial direction, which

decreases the axial velocity along the downstream across the LPF.

4.4. Emission Formation

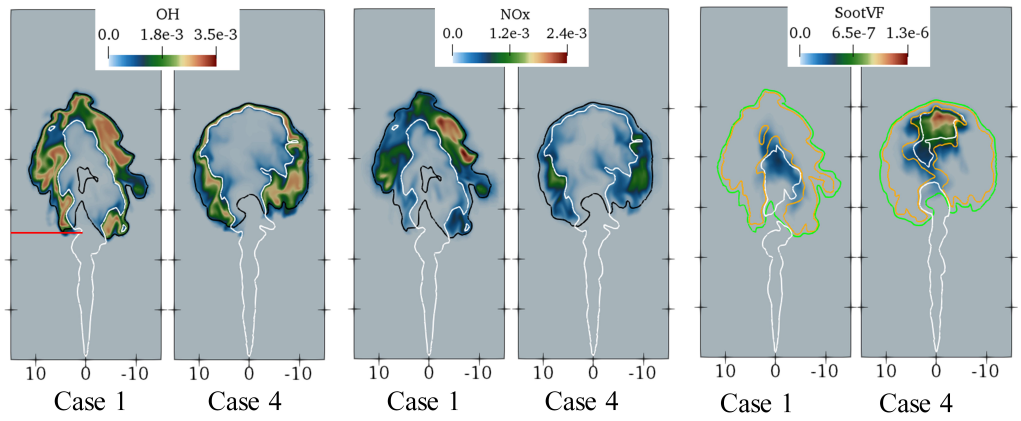

Figure 11: Instantaneous distributions of the mass fractions of OH radicals and NOx, and soot volume fraction (SootVF) at time of τ_{ig} + 0.5 ms. OH: white line: $\Phi = 1.3$; black line: temperature of 1800 K; red line: liftoff length from experiment [30]. NOx: white line: $\Phi = 1.3$; black line: temperature of 1800 K. Soot volume fraction: white line: temperature of 1600 K; green line: temperature of 2200 K; yellow line: $\Phi = 2$.

Fig. 11 shows the instantaneous fields of mass fractions of OH and NOx, and the soot volume fraction, SootVF. OH is found in the mixture of $\Phi < 1.5$. The region of high NOx overlaps with the high OH region. In Case 4, due to the presence of LPF, the OH and NOx regions at the spray tip are rather thin; thus, the production of NOx in the RCCI case is lower than that in the single fuel case, Case 1. Soot is shown to be generated in the region of $\Phi > 2$ and temperature between 1600 K and 2200 K, consistent with Ref. [38]. A larger soot zone is shown at the central fuel-rich region close to the spray tip in the RCCI case, whereas the single-fuel case, Case 1, exhibits a significantly smaller soot region and a lower

soot volume fraction. This is well consistent with the mixing field shown in Fig. 9.

5. Conclusions

The combustion characteristics and NOx/soot formation in n-heptane spray flames in a constant volume combustion vessel, under conditions relevant to the low temperature reform (LTR) gas reactivity controlled compression ignition (RCCI) combustion, is studied using large eddy simulations with a transported probability density function (PDF) sub-grid scale model. The spray model and LES-PDF combustion model are validated against ECN Spray-H experimental results. Very good agreement between the LES results and experiments is obtained for the spray liquid length, vapor fuel penetration length, mixture fraction profile, pressure rise profile, ignition delay time (IDT), and liftoff length (LOL). The LES results are used to analyze the combustion and emission process. The following conclusions are drawn.

The IDT of the spray and the LOL of the spray flame are sensitive to the LTR gas composition, thus, to the LTR temperature (reform temperature). Both the IDT and LOL increase with increasing LTR temperature, due to the decreasing effect of cool flame in the n-heptane ignition process. The reaction zone structure in the RCCI case is significantly different from that of the n-heptane spray flame case. The RCCI case exhibits a double-layer flame structure at the spray tip and in the periphery of spray flame, consisting of a mixing-controlled diffusion flame (DF) layer and a lean premixed flame (LPF) layer on the lean side of DF. The presence of LPF affects the mixing process around the spray tip, resulting in a much lower NOx production at the flame tip. However, the fuel-rich region upstream of the flame

tip is larger in the RCCI case, which results in a higher level of soot formation.

Acknowledgments

This work was supported by National Natural Science Foundation of China No. 51876139 and No. 51676136, and the Swedish Research Council (VR). SZ and SX acknowledge the support from the China Scholarship Council. The simulations were performed on resources provided by the Swedish National Infrastructure for Computing (SNIC) at HPC2N and NSC.

References

[1] R. D. Reitz, G. Duraisamy. Review of high efficiency and clean reactivity controlled compression ignition (RCCI) combustion in internal combustion engines, Progress in Energy and Combustion Science 46 (2015) 12–71.

[2] L. Tartakovsky, M. Sheintuch. Fuel reforming in internal combustion engines, Progress in Energy and Combustion Science 67 (2018) 88–114.

[3] C. Geng, H. Liu, Y. Cui, Z. Yang, X. Fang, L. Feng, M. Yao. Study on single-fuel reactivity controlled compression ignition combustion through low temperature reforming, Combustion and Flame 199 (2019) 429–440.

[4] L. Xu, X.-S. Bai, M. Jia, Y. Qian, X. Qiao, X. Lu. Experimental and modeling study of liquid fuel injection and combustion in diesel engines with a common rail injection system, Applied energy 230 (2018) 287–304.

[5] L. Xu, X.-S. Bai, Y. Li, M. Treacy, C. Li, P. Tunestål, M. Tunér, X. Lu. Effect of piston bowl geometry and compression ratio on in-cylinder combustion and engine performance in a gasoline direct-injection compression

ignition engine under different injection conditions, Applied Energy 280 (2020) 115920.

[6] A. Tsolakis, A. Megaritis, M. Wyszynski. Low temperature exhaust gas fuel reforming of diesel fuel, Fuel 83 (2004) 1837–1845.

[7] T. Alger, B. Mangold. Dedicated egr: a new concept in high efficiency engines, SAE international journal of engines 2 (2009) 620–631.

[8] J. Cho, S. Park, S. Song. The effects of the air-fuel ratio on a stationary diesel engine under dual-fuel conditions and multi-objective optimization, Energy 187 (2019) 115884.

[9] S. Zhong, F. Zhang, Q. Du, Z. Peng. Characteristics of reactivity controlled combustion with n-heptane low temperature reforming products, Fuel 275 (2020) 117980.

[10] Z. Wang, J. Abraham. Fundamental physics of flame development in an autoigniting dual fuel mixture, Proceedings of the Combustion Institute 35 (2015) 1041–1048.

[11] E. Demosthenous, G. Borghesi, E. Mastorakos, R. S. Cant. Direct numerical simulations of premixed methane flame initiation by pilot n-heptane spray autoignition, Combustion and Flame 163 (2016) 122–137.

[12] S. Hu, C. Gong, X. S. Bai. Dual fuel combustion of n-heptane/methanol-air-egr mixtures, Energy Procedia 105, 4943-4948 105 (2017) 4943–4948.

[13] A. Srna, B. von Rotz, M. Bolla, Y. M. Wright, K. Herrmann, K. Boulouchos, G. Bruneaux. Experimental investigation of pilot-fuel combustion in dual-

fuel engines, part 2: Understanding the underlying mechanisms by means of optical diagnostics, Fuel 255 (2019) 115766.

[14] H. Kahila, A. Wehrfritz, O. Kaario, V. Vuorinen. Large-eddy simulation of dual-fuel ignition: Diesel spray injection into a lean methane-air mixture, Combustion and Flame 199 (2019) 131–151.

[15] H. Wei, W. Zhao, J. Qi, Z. Liu, L. Zhou. Effect of injection timing on the ignition process of n-heptane spray flame in a methane/air environment, Fuel 245 (2019) 345–359.

[16] P. Rosin. Laws governing the fineness of powdered coal, Journal of Institute of Fuel 7 (1933) 29–36.

[17] M. Jangi, R. Solsjo, B. Johansson, X.-S. Bai. On large eddy simulation of diesel spray for internal combustion engines, International Journal of Heat and Fluid Flow 53 (2015) 68–80.

[18] A. Hadadpour, M. Jangi, K. M. Pang, X. S. Bai. The role of a split injection strategy in the mixture formation and combustion of diesel spray: A large-eddy simulation, Proceedings of the Combustion Institute 37 (2019) 4709–4716.

[19] R. D. Reitz. Modeling atomization processes in high-pressure vaporizing sprays, Atomisation Spray Technology 3 (1987) 309–337.

[20] C. Gong, M. Jangi, X.-S. Bai. Large eddy simulation of n-dodecane spray combustion in a high pressure combustion vessel, Applied energy 136 (2014) 373–381.

[21] L. Valino. A field monte carlo formulation for calculating the probability density function of a single scalar in a turbulent flow, Flow, turbulence and combustion 60 (1998) 157–172.

[22] C. Dopazo. Relaxation of initial probability density functions in the turbulent convection of scalar fields, The Physics of Fluids 22 (1979) 20–30.

[23] W. Jones, A. Marquis, V. Prasad. Les of a turbulent premixed swirl burner using the eulerian stochastic field method, Combustion and Flame 159 (2012) 3079–3095.

[24] M. Jangi, X.-S. Bai. Multidimensional chemistry coordinate mapping approach for combustion modelling with finite-rate chemistry, Combustion Theory and Modelling 16 (2012) 1109–1132.

[25] G. Wanner, E. Hairer, Solving ordinary differential equations II, Springer Berlin Heidelberg, 1996.

[26] T. Lu, C. K. Law, C. S. Yoo, J. H. Chen. Dynamic stiffness removal for direct numerical simulations, Combustion and Flame 156 (2009) 1542–1551.

[27] A. Williams, M. Pourkashanian, P. Bysh, J. Norman. Modelling of coal combustion in low-nox pf flames, Fuel 73 (1994) 1006–1019.

[28] K. M. Leung, R. P. Lindstedt, W. Jones. A simplified reaction mechanism for soot formation in nonpremixed flames, Combustion and flame 87 (1991) 289–305.

[29] H. Jasak, A. Jemcov, Z. Tukovic, et al., in: International workshop on coupled

methods in numerical dynamics, volume 1000, IUC Dubrovnik Croatia, pp. 1–20.

[30] L. Pickett, G. Bruneaux, R. Payri. Engine combustion network, Sandia National Laboratories, Livermore, CA, http://www.ca.sandia. gov/ecn (2014).

[31] S. Xu, K. M. Pang, Y. Li, A. Hadadpour, S. Yu, S. Zhong, M. Jangi, X.-S. Bai. Les/tpdf investigation of the effects of ambient methanol concentration on pilot fuel ignition characteristics and reaction front structures, Fuel 287 (2021) 119502.

[32] H. J. Curran, P. Gaffuri, W. J. Pitz, C. K. Westbrook. A comprehensive modeling study of n-heptane oxidation, Combustion and flame 114 (1998) 149–177.

[33] S. Som, D. E. Longman, Z. Luo, M. Plomer, T. Lu, P. K. Senecal, E. Pomraning. Simulating flame lift-off characteristics of diesel and biodiesel fuels using detailed chemical-kinetic mechanisms and large eddy simulation turbulence model, Journal of energy resources technology 134 (2012).

[34] S. Xu, S. Zhong, K. M. Pang, S. Yu, M. Jangi, X.-S. Bai. Effects of ambient methanol on pollutants formation in dual-fuel spray combustion at varying ambient temperatures: A large-eddy simulation, Applied Energy 279 (2020) 115774.

[35] D. Hariharan, R. Yang, Y. Zhou, B. Gainey, S. Mamalis, R. E. Smith, M. A. Lugo-Pimentel, M. J. Castaldi, R. Gill, A. Davis, et al. Catalytic partial oxidation reformation of diesel, gasoline, and natural gas for use in low temperature combustion engines, Fuel 246 (2019) 295–307.

[36] F. Liu, Z. Shi, Z. Zhang, Y. Li, C. Sun. Numerical study on critical ambient temperature for auto-ignition of the diesel spray under cold-start conditions, Fuel 258 (2019) 116191.

[37] L. Xu, X.-S. Bai, C. Li, P. Tunestål, M. Tunér, X. Lu. Combustion characteristics of gasoline dici engine in the transition from hcci to ppc: Experiment and numerical analysis, Energy 185 (2019) 922–937.

[38] J. E. Dec. Advanced compression-ignition engines - understanding the in-cylinder processes, Proceedings of the combustion institute 32 (2009) 2727–2742.